Precision Engineering 67 (2021) 58–68

Contents lists available at ScienceDirect

Precision Engineering

journal homepage: http://www.elsevier.com/locate/precision

Build position-based dimensional deviations of laser powder-bed fusion of stainless steel 316L

Jithin Kozhuthala Veetil [a], Mahyar Khorasani [a,b,*], AmirHossein Ghasemi [d], Bernard Rolfe [b], Ivo Vrooijink [c], Karin Van Beurden [c], Sebastiaan Moes [c], Ian Gibson [a,b]

[a] Fraunhofer Project Centre for Complex System Engineering, Department of Design, Production, and Management, University of Twente, Enschede, the Netherlands
[b] School of Engineering, Deakin University, Waurn Ponds, Victoria, Australia
[c] Saxion University, Enschede, the Netherlands
[d] Department of Manufacturing and Production, University of Kashan, Iran

ARTICLE INFO

Keywords:
Additive manufacturing
Assist gas pressure
Dimensional deviations
Powder bed fusion
Grain size

ABSTRACT

This study investigates the effect of position on build-plate on the dimensional deviations for stainless steel 316 L samples made by laser powder-bed fusion. To understand the effect of sample position on the build-plate (substrate) with respect to shrinkage and dimensional deviation, 36 samples in a 6 × 6 array were printed with three repetitions. The value of the diameter was measured at 10 points along the vertical axis in the perpendicular and parallel directions to the flow of the assisted gas. The results of the experiment show that there is shrinkage in both directions with respect to the gas flow. However, the extent of deviation in the perpendicular direction to the gas flow is greater compared to the parallel diameters for the samples. This can be related to the pressure of assisted gas and the difference in cooling rate corresponding to the position of the samples on the building substrate. The hypothesis is proved by conducting further experiments regulating the amount of gas flow by adjusting the individual nozzle for the gas flow to the build chamber. The reason for these deviations is speculated to be related to the rheology of the melt pool. This research could lay a solid foundation for the future development of a compensation strategy to nullify the effect of shrinkage and dimensional deviations on parts made using the laser powder-bed fusion technique. The results of shrinkage of the columns appear to suggest that there is an effect on the circularity from the assisting gas.

1. Introduction

Many believe that there is a disruption occurring to conventional metal manufacturing processes since the introduction of advanced manufacturing techniques. The adoption of these advanced technologies in manufacturing helps to deliver products with a high level of design and technically complex products that need to be reliable and readily available. Additive manufacturing (AM) is the technology that builds 3D shapes by stacking layer upon layer of a material, which can be plastic, metal, composite, concrete, or even human tissue. Seven classifications in AM were introduced by Gibson et al. [1], and Laser Powder Bed Fusion (LPBF) is one of the most common printing techniques used to print metals parts. In a laser powder bed fusion process, thin layers of powder are applied to a build plate, and a laser beam is used to fuse the powder at locations specified by the model of desired geometry. When one layer is completed, a new layer of powder is applied, and the process is repeated until a 3D part is produced. Metal LPBF parts have anisotropic mechanical properties compared to the parts made from conventional manufacturing [2]. While printing a metal part using the LPBF process, each fused layer undergoes several cycles of rapid melting followed by cooling and solidification. This plays a significant role in determining the quality and properties of the end product. Porosity, warpage, residual stress, and cracking are a few of the significant issues for powder-based AM systems faced during printing metal parts [3]. These factors directly or indirectly contribute to the shrinkage or dimensional deviation of the finished parts. Rapid melting and solidification of powder in AM processes are accompanied by shrinkage in the metal volume. This shrinkage in the volume is the critical reason for the

* Corresponding author. Department of Design, Production, and Management, University of Twente, Enschede, the Netherlands.
E-mail addresses: j.kozhuthalaveetil@utwente.nl (J.K. Veetil), a.khorasani@deakin.edu.au (M. Khorasani), amir_hosein_ghasemi2012@yahoo.com (A. Ghasemi), Bernard.rolfe@deakin.edu.au (B. Rolfe), i.b.e.vrooijink@saxion.nl (I. Vrooijink), k.m.m.vanbeurden@saxion.nl (K. Van Beurden), s.moes@saxion.nl (S. Moes), i.gibson@utwente.nl (I. Gibson).

https://doi.org/10.1016/j.precisioneng.2020.09.024
Received 22 April 2020; Received in revised form 21 September 2020; Accepted 26 September 2020
Available online 28 September 2020

Table 1
Chemical composition of the powder.

COMPONENT	FE	CR	NI	MO	MN	SI	P	C	S
INDICATIVE VALUE (%)	**Balance**	17	12.2	2.25	1.8	0.65	0.040	0.030	0.030

lack of build quality in terms of dimensional accuracy, especially in assembly of components [4].

Some investigations have focused on shrinkage and dimensional deviations of AM parts. Ameta et al. [5] have studied the tolerance specification and related issues in AM. The main topic of their study is the tolerance specification based on build direction and location, layer thickness, and support structure. They concluded that AM has a strong need for additional standards that ensure better dimensional accuracy for the parts made. Within metal AM, Alvarez et al. [6] have used a procedure known as inborn shrinkage, previously created for multi-pass welding forms, to predict the distortion of LPBF parts made by Inconel 718. Chen et al. [7] used CFD simulations to study the flow of assisted gas inside the build chamber and found out that CFD could help to improve the product quality by reducing porosity. However, they did not investigate the effect on shrinkage, in particular the shrinkage in the direction of the gas flow. Królikowski and Filipowicz [8] presented a unique approach for the accurate measurement of LPBF metal parts with thin walls. The focus of this experiment was to find the influence of thin-walled geometric entities and the placement of these entities on the overall build accuracy using a CMM. The results showed that there were deviations; however, no significant dependency could be verified from the measured results. Kamarudin et al. [9] studied the feasibility of LPBF by investigating the surface roughness and dimensional accuracy of a number of parts built on a single build plate using constant process parameters. They found that the values of surface roughness on the bottom are higher than the top and side of the benchmark. This is related to the thermal conductivity of the substrate on the first layers. However, they did not explore the correlation of where the parts were on the build plate with respect to the direction of the assisted gas flow. Zhang et al. [10] proposed a theoretical model to predict the dimensional accuracy specifically for horizontal dimensions of LPBF (where the vertical direction is in the build direction by definition). They found out that horizontal dimensional accuracy for LPBF consists of two parts: first is based on the mode of track filling, and the other is based on the width of the tracks. The developed model shows promising results when the samples have smooth surfaces or surfaces with cavities; however, the model has less success when the samples have surfaces with balling effects. Wang et al. [11] studied the characteristics for typical geometric features made by LPBF and concluded that the main factors that influenced the geometry for metal parts are optical spot diameter, laser penetration, powder adhesion, and the stair-case effect. Shukri et al. [12] proposed and validated two distortion compensation approaches (1: Finite Element Analysis-based; and 2: Optical 3D scan based) on a turbine blade component, and the authors have successfully compensated distortion for industrial LPBF parts. Yang et al. [13] studied the optimization strategy for shape accuracy for stainless steel 316 L for custom orthodontic productions. The results provide the optimal process parameters to fabricate precisely customized structures.

In the current work, shrinkage of built columns based on the position of the samples on the build plate relative to the direction of the assisted gas was investigated. Various printing strategies, including full and customized assisted gas pressures, were carried out to find the effect of the gas on the dimensional deviations. Diameters of built columns were measured with respect to the perpendicular and parallel direction of the flow of the assisted gas. The deviations are speculated to be linked to the flow of inert gas and rheological phenomena of the melt pool. Finally, this work suggests the assisted gas has some effect on shrinkage and dimensional deviations.

Table 2
Shows the LPBF parameters and specifications which kept constant based on original equipment manufacturer (OEM) recommendations.

System Parameters	Value
Laser power	90 W
Scanning speed	1500 mm/s
Min. Scan-Line/Wall Thickness	120 μm
Operational Beam Focus diameter	50 μm
layer thickness	30 μm

2. Experimental setup

2.1. Powder material and LPBF process

Gas atomized CL 20 ES stainless steel 316 L (austenitic chromium-nickel) was supplied by Concept Laser for the experiment. The CL 20 ES powder was subjected to various analyses such as tensile tests at 20 °C according to DIN EN 50125 and hardness test, according to DIN EN ISO 6508. The material was analyzed and checked by an external and independent testing laboratory for chemical analysis that is shown in Table 1. The standard process parameters used for printing the samples are given in Table 2. Fig. 1(A) shows the particle distribution for feedstock used in this experiment. The CL 20 ES powder used for the experiment is sieved using "Retsch AS 200″ vibratory sieve shaker since the powder was already used for previous builds in the Concept Laser machine.

CAD generated cylindrical models were designed in SolidWorks with a diameter of 10 mm. 36 samples in a 6 × 6 array were printed with three repetitions for each build job. The layout of the samples on the build plate is shown in Fig. 1(B). Based on the arrangement of samples on the build-plate, row 6 (Samples 31–36) is closest to the chamber window, and row 1 (samples 1–6) is the farthest from the chamber window. Furthermore, column 1 (Samples 1–31) is farthest from the inert gas inlet vent, and column 6 (Samples 6–36) is closest to the inert gas inlet vent. Samples from the build plate were cut out using wire cut electric discharge machine. The scanning order for different samples was stochastic, and the place of the inert gas nozzles and the flow of the gas is shown in Fig. 1(C). Assisted gas is argon and blown from six nozzles in the right-hand side of the chamber with a pressure of 2 bar.

3. Diameter measurement

The shrinkage of the samples was observed by measuring the diameter at 10 points along with the height at intervals of approximately 1 mm. In order to remove the effects of the attached powder particles, the samples were cleaned using an ultrasonic method for 30 min. The device used for measuring the sample diameter was a micrometer screw gauge with 1 μm resolution installed on the measurement stand. To fully evaluate the shrinkage value, the diameter was measured in two different directions comprising of perpendicular and parallel directions of the flow to the assisted gas (Fig. 2). Specific latex gloves were used while measuring the samples to reduce the transfer of temperature or any other kind of contamination from the hand. The lab temperature and humidity were maintained at 20 °C and 30%, respectively, to have maximum consistency for all measurements.

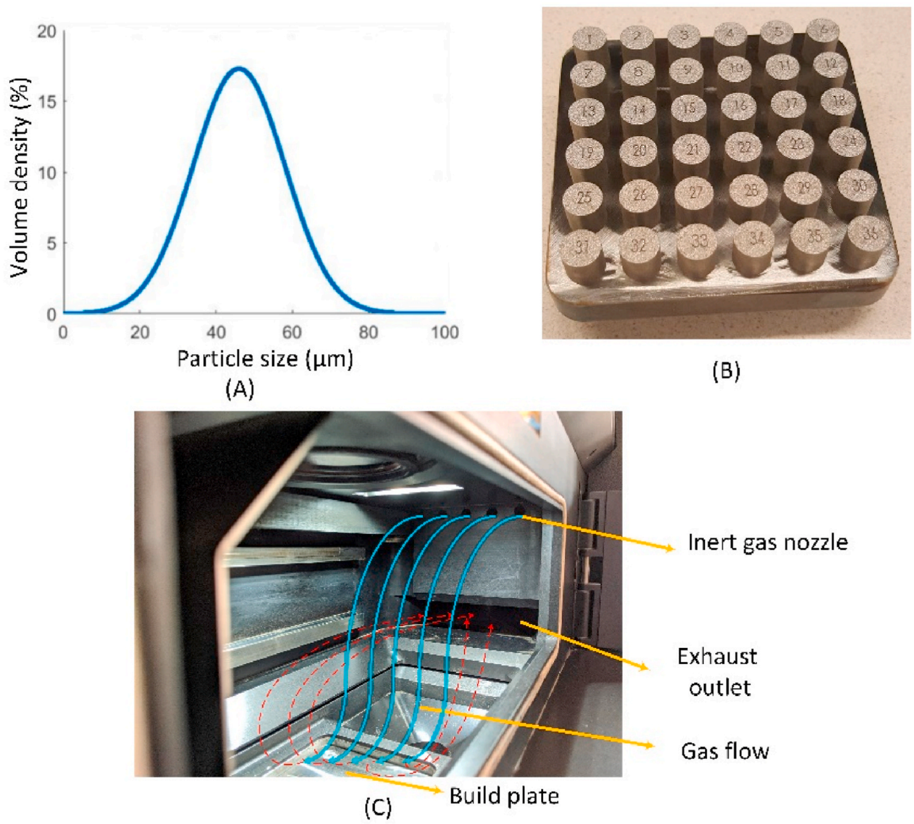

Fig. 1. (A) Particle distribution of CL 20 ES Stainless Steel, (B) Layout of samples in the build plate, (C) Schematic of the assisted gas flow within the build chamber (The red lines show the return path which is very close to the side walls). (For interpretation of the references to colour in this figure legend, the reader is referred to the Web version of this article.)

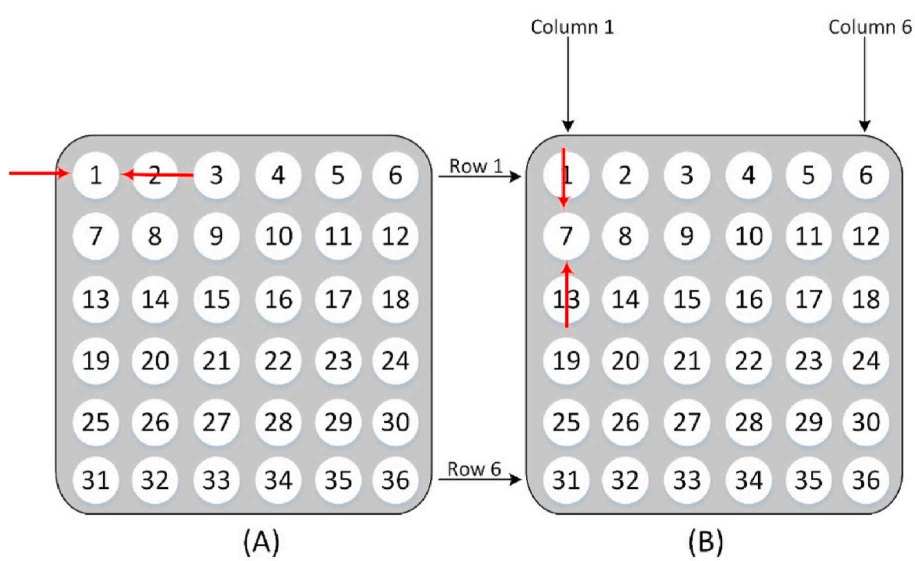

Fig. 2. (A) Parallel and (B) Perpendicular diameter measurement directions relative to the build plate.

4. Results

4.1. Dimensional results in rows

Concept laser machines add 5% to the nominal dimensions from the CAD model; this is due to solidification and shrinkage effects (reduction in dimensions). Therefore, when printing samples with a 10 mm diameter, the real diameter that is printed by the machine is 10.5 mm. After printing, the samples were cleaned with high-pressure airflow and a soft brush. The perpendicular and parallel diameters for all 108 samples are found out to be in the range of 10.07 and 10.12 mm. The dimensional deviation was calculated by comparing the obtained values and nominal diameter (10 mm), and shrinkage was calculated by comparing the obtained values and real print diameter (10.5 mm).

Fig. 3 shows that the average perpendicular diameter for samples 1–6 through to 31–36 overall showed a decreasing trend. The average

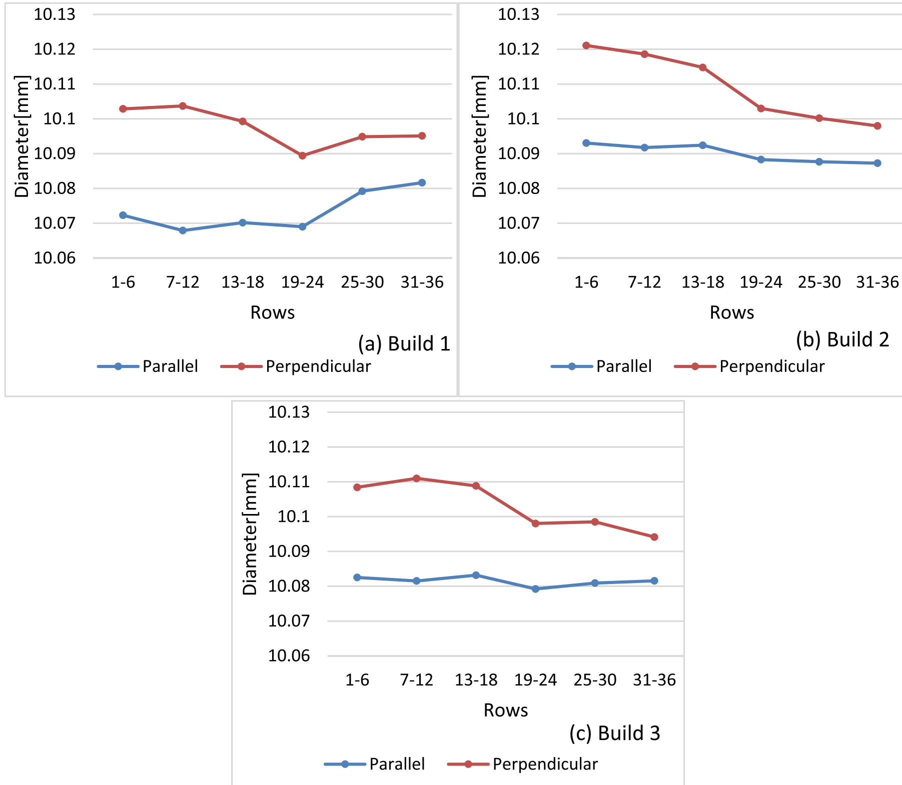

Fig. 3. Average row sample diameters in parallel and perpendicular directions (a) Build 1, (b) Build 2, and (c) Build 3.

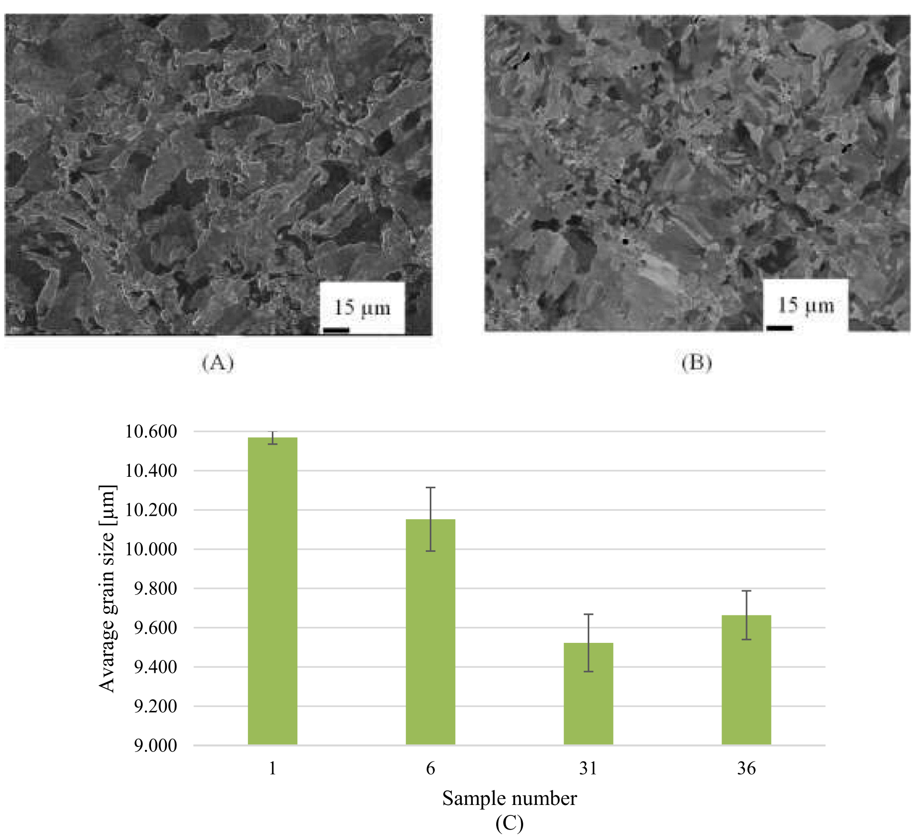

Fig. 4. SEM images for (a) sample 6 (b) sample 31 and (C) Average grain size for samples 1, 6, 31, and 36.

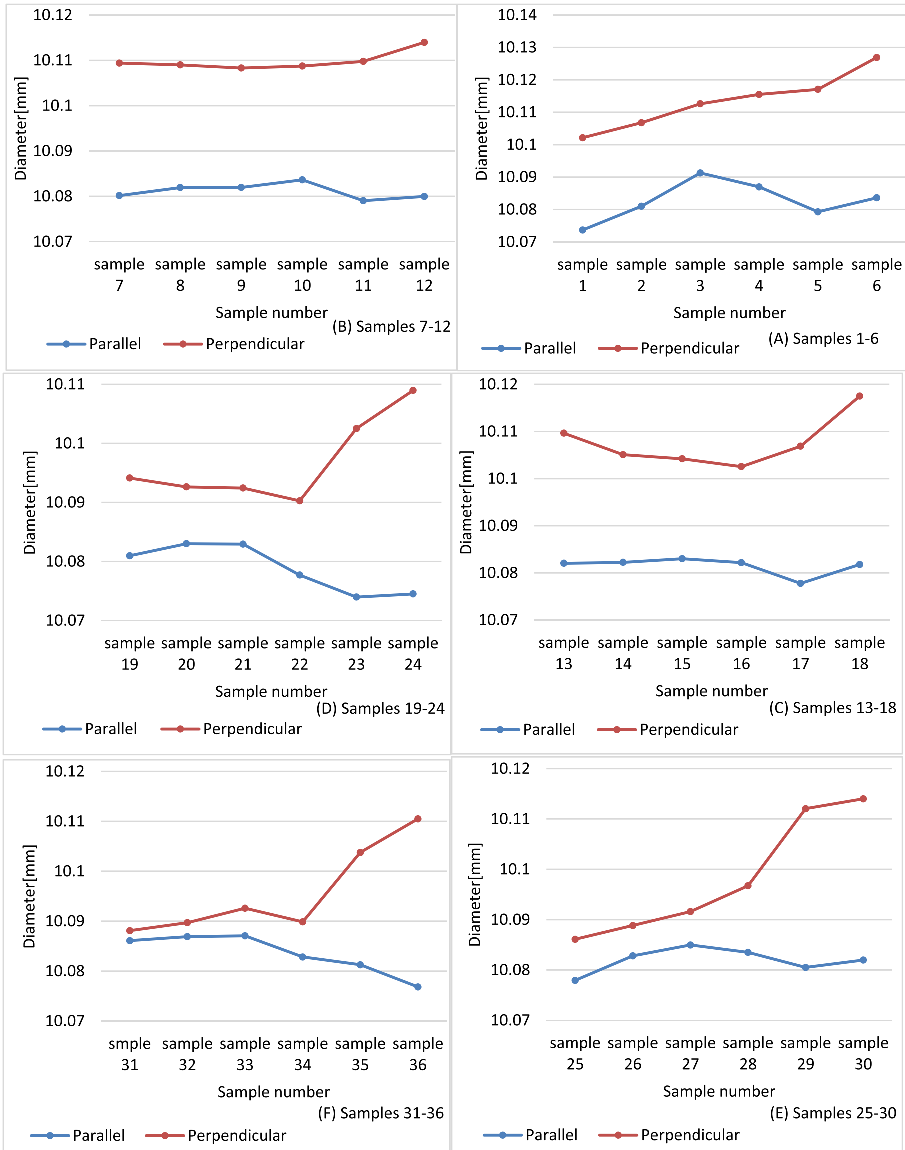

Fig. 5. Average perpendicular and parallel diameter of the samples across the three builds.

parallel diameter for samples 1–6 through to 31–36 is found out to have a more stable value. This means that overall the samples had decreasing dimensional deviations from the top to the bottom of the build plate. The authors speculate that this is related to the difference in the temperature and cooling within the build print area. The last rows (31–36) are close to the window and chamber door, which may have cooler conditions (perhaps due to atmospheric conduction). In the last row (close to the chamber door), the time of solidification is lower than the first rows due

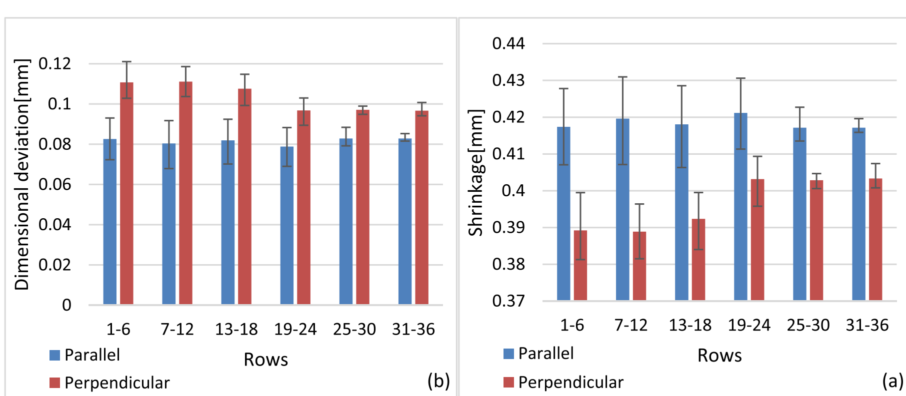

Fig. 6. Average (a) Shrinkage (b) Dimensional deviation in each row.

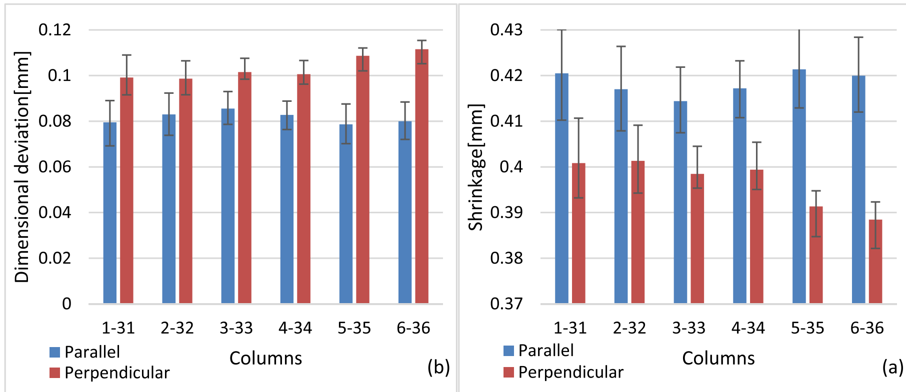

Fig. 7. Average (a) Shrinkage (b) Dimensional deviation in each column.

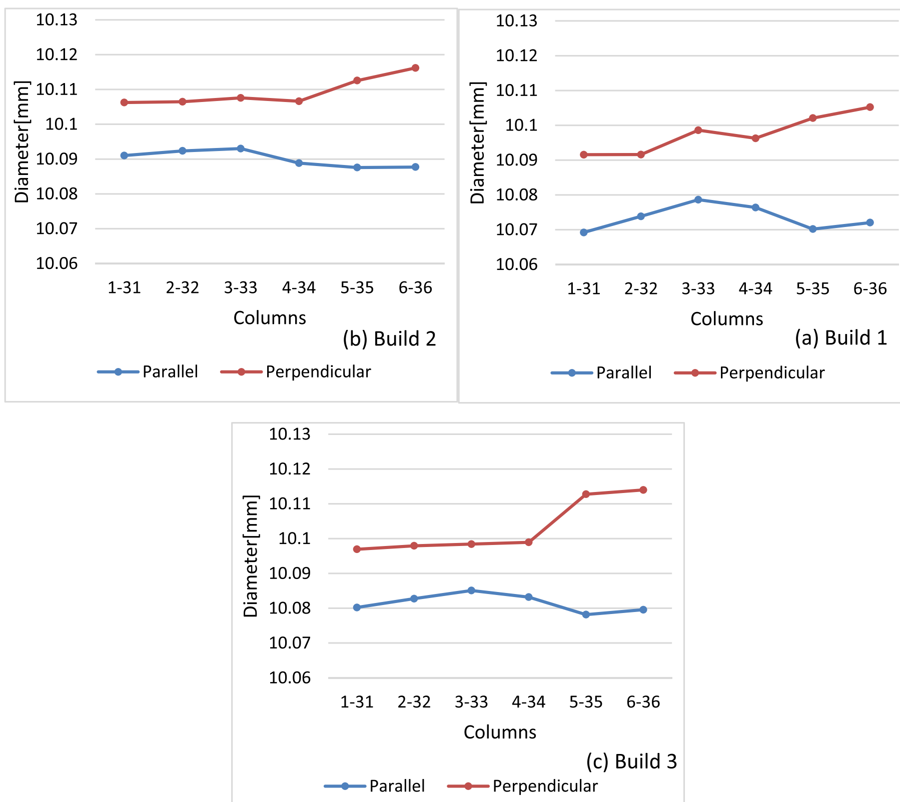

10

Fig. 8. Average column sample diameters for parallel and perpendicular for the three repetitions (a) Build 1, (b) Build 2 and (c) Build 3.

to a higher cooling rate. The evidence for this can be seen in the SEM images that show a smaller cross-sectional grain size for sample 31 compared to sample 6. The SEM images show the cross-section of the samples, which is perpendicular to building direction; thus, the grains are typically a combination of equiaxed and short columnar grains. The long columnar grains are formed in the build direction. Therefore, the intercept method can provide an estimation of the cross-sectional grain size. This provides some evidence for the authors' proposed hypothesis [14]. Fig. 4(A) and (B) show the SEM images of the samples 6 and 31.

However, when the deviations for each row were investigated, it is found that the right-hand side columns had higher dimensional deviations than on the left, as shown in Fig. 5. The authors hypothesize that this may be related to the effect of assisted gas during the build on these columns. Also, it is interesting to note that the larger diameter is always formed in the perpendicular direction compared to the parallel diameter (Fig. 5). It shows that the atmospheric conduction of the window may be dominating the convection response, however locally, convection is causing an increase in the perpendicular diameter.

The average diameters and dimensional deviations for all three build plates are shown in Fig. 6. The difference between the parallel and perpendicular results for a given sample provides an estimate of the circularity of the sample; that is, smaller, the difference between the parallel and perpendicular measurements higher the circularity. The trend for the row diameters in this figure shows that the difference between both the parallel and perpendicular diameters for samples that are printed at the bottom of the build plate (samples 31 to 36) are smaller

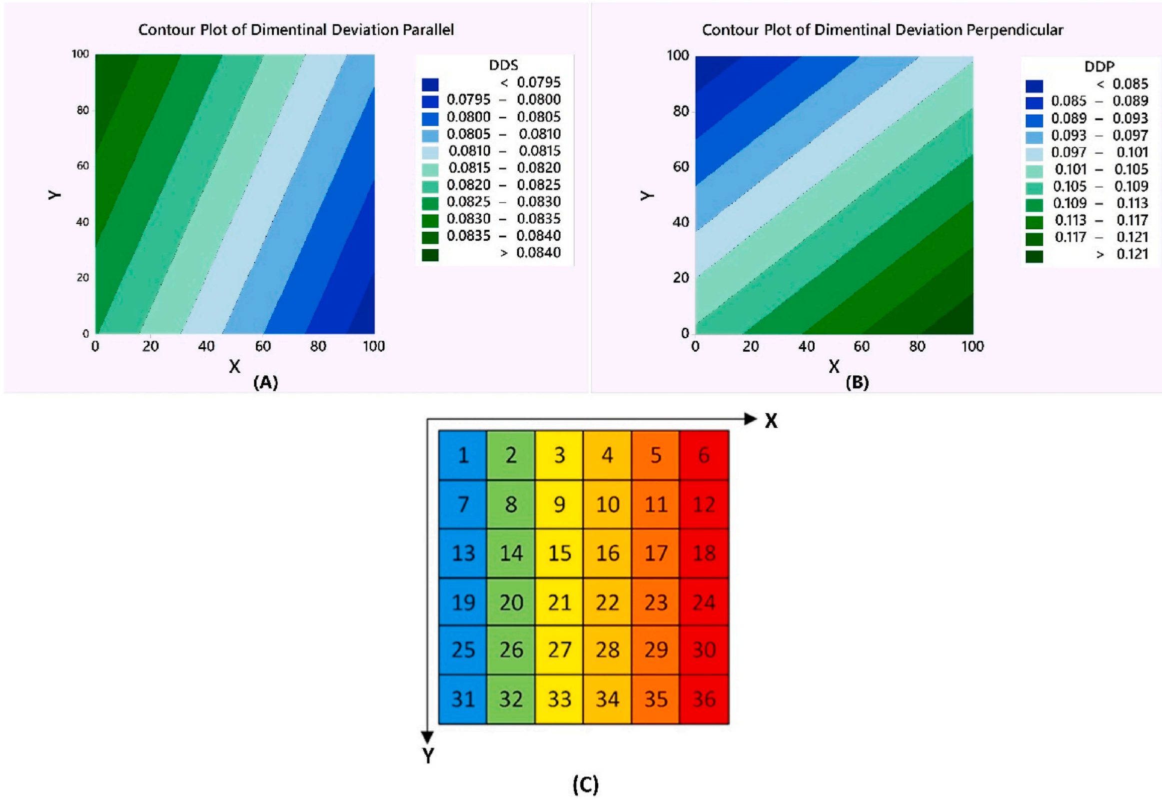

Fig. 9. Contour plot of dimensional deviations for (A) Parallel (B) Perpendicular (C) Substrate position mapping, DDP is Dimensional Deviation in Perpendicular, and DDS is Dimensional Deviations in Parallel diameters.

(potentially more circular). The results of this figure are in agreement with Figs. 3 and 5 and the grain size analysis. The results in Fig. 6 also show that the parallel results (blue) are relatively stable, while the perpendicular results (red) show there is a change in their results between the first three rows relative to the last three rows.

4.2. Dimensional results in columns

Fig. 7 shows the samples that are printed in the first column (samples 1–31) have lower dimensional deviations in perpendicular diameter, which can be related to the effect of the cooling rate. The authors suggest that the effect of assisted gas is less for the left columns compared to the columns on the rightmost side. Therefore, for the samples 6 to 36, the difference between diameters specifically for perpendicular direction is higher (Fig. 7). This may show the local effect of the gas from left to right (relative to the build plate).

From Fig. 8, it can be seen that both diameters are closer for the left columns (first three columns), which shows a reduction in the dimensional deviation. The contour plots in Fig. 9 (A and B) show that the parallel deviation appears to be varying with the horizontal position on the build plate, and the overall change is small. In contrast, the perpendicular deviation appears to be affected by the horizontal and vertical position. Samples 6 and 31 show the maximum and minimum deviation for perpendicular diameters, respectively.

The error bars in Fig. 7 show that the mean and standard deviation for all samples in parallel and perpendicular directions are within an acceptable print accuracy range. Less than a 5% error was found and proves excellent repeatability for sample production. The next section will discuss these observed results and speculate about the reasoning for why the observed correlations were seen.

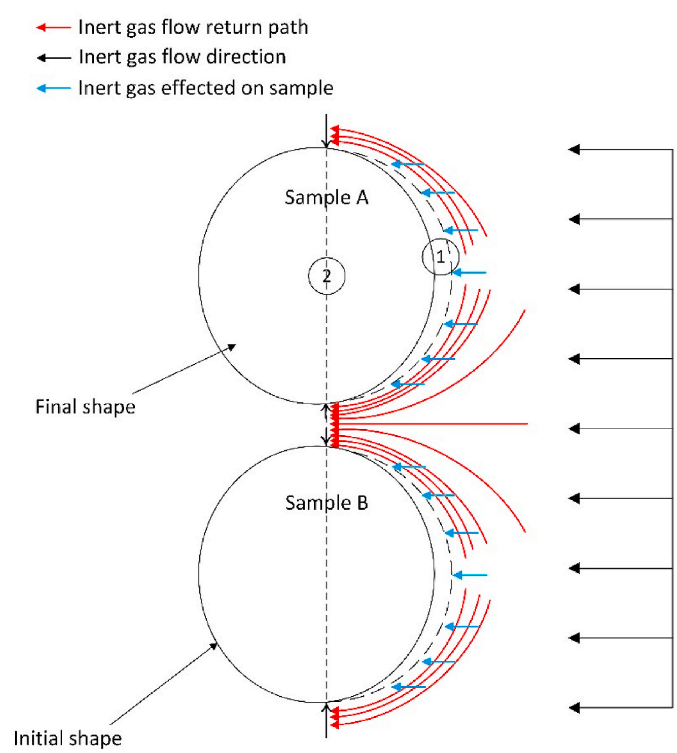

Fig. 10. Effect of blowing assisted gas across the samples.

5. Verification and discussion

5.1. Discussion

Results show that all samples are elliptical, which the authors believe could be related to the flow of the assisted gas across the melt pool. This can be related to the pressure of the gas that leads to heterogeneous solidification. Along the gas direction, the melting area diverges from the nominal position. According to Fig. 10, the flow of the gas turns/moves/passes around or from the top of the samples. The gas would act as a driving force for solidification in one direction and pushes the bottom and upper side of the melting area and result in the smaller diameter along flow direction (parallel) and a larger perpendicular diameter. The convective effect of gas on solidification causes samples to have higher undercooling, increased heat transfer rate, and heterogeneous solidification [15–17].

It is reported [18] that the numerically calculated cooling rate decreases from 6548 K/s to 2779 K/s using an analytical heat condition model from the first to the third layers, and this is related to the periodic heating effect and the further distance from the substrate in LPBF system. Therefore, a wider mush area is generated for the top layers, and reaction forces on the samples make inconsistency in perpendicular diameter along blowing gas. However, the reaction force rebounds against the gas and forms a constant diameter in a parallel direction.

LPBF is a thermal-based method, so melting and solidification periodically happen in a fraction of a second. Therefore, temperature from the previous layers are accumulated in the samples, and the heterogeneous (non-uniform) force from assisted gas produces elliptic samples.

The pressure of the assisted gas is 2 bar and is blown on the surface from six nozzles in the right-hand side of the build chamber. The direction of gas flow is towards the center of the build chamber, where it then changes direction to flow across the build plate and into the exhaust vent. Heat transfer is affected by repeated heating of the lower printed layers (power bed conduction) and convection effects from the assisted gas. Therefore, due to the divergence effect of the assisted gas and the reduction in speed and pressure in the farthest left spot of the substrate, there was less dimensional deviation observed, and the samples have better circularity.

In the PBF process, due to constant pressure in the working chamber, the value of surface tension for lower than critical (boiling) temperature is obtained from Equation (1).

$$\gamma = \gamma^{*}\left[\frac{T_C - T_0}{T_C}\right]\left[1 - \frac{T - T_0}{T_C - T_0}\right]^{n} \tag{1}$$

where γ^{*} is constant for each liquid, T_c and T_0 are a reference, and critical temperature and n is an empirical ratio that is related to the experimental situation. From a rheological point of view, when the temperature is changed, the surface tension and work of adhesion will change.

Equation (1) is called the thermocapillary effect and suggests that an increased temperature decreases the surface tension. Surface tension is the resistance of the surface against external forces, therefore in the area of higher temperature (rightmost rows on the build plate), higher dimensional deviations are expected. Fig. 9 shows that with a higher cooling rate and lower temperature, both parallel and perpendicular diameters are formed with closer values and therefore generate less dimensional deviation.

Another reason the authors believe that the higher dimensional deviation is related to a work of adhesion which is a rheological phenomenon. The work of adhesion is defined for solid, liquid, or solid/liquid phases. In solid-liquid interfaces such as melt pool and previous layer, the surface energy is defined from Equation (2).

$$E_{SL} = \gamma_{SL}\, S_C \tag{2}$$

where E_{SL} is the surface energy in solid-liquid interphase and S_c in the area of contact between solid and liquid phases. The energy and work that is required to separate the melting pool and solidified layer are obtained from Equation (3) [19,20].

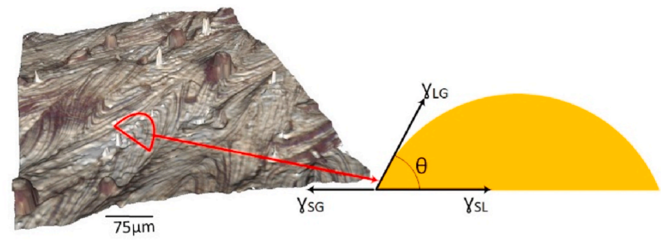

Fig. 11. Triple contact line on the solidified melting pool.

$$E_t = E_1 + E_2 = (\gamma_1 + \gamma_2)S_C \tag{3}$$

$$W_a = \gamma_1 + \gamma_2 - \gamma_{12}$$

$$\gamma_1 = \gamma_{LG}\ ,\ \gamma_2 = \gamma_{SG}\ , \gamma_{12} = \gamma_{SL}$$

Fig. 11 shows the triple contact line on the layered surface. By considering static situation (due to not observing Rayleigh instability and balling effect) on the topmost surface at equilibrium temperature, the forces along scan direction should be zero. Therefore, the work of adhesion is obtained according to Equation (4).

$$\gamma_{SL} COS\theta = \gamma_{SG} - \gamma_{SL} \tag{4}$$

$$W_a = \gamma_{LG}(1 + \cos\theta)$$

For the samples which were printed in the top three rows (rows 1–3), the cooling rate is comparatively less, and due to the thermocapillary effect, the value of the surface tension and subsequent work of adhesion reduces. Therefore, less adhesion force is generated between the melting pool and previously solidified layer as a result of higher temperatures. In this situation, assisted gas pushes the melt pool, which has less adhesion resulting in higher dimensional deviations in perpendicular diameter.

5.2. Assisted gas adjustment

To verify the effect of the assisted gas on dimensional deviation, two sets of samples similar to previous builds (cylindrical samples with a diameter of 10 mm) were printed, keeping all the process parameters the same as the previous process. The only variation from the previous build is the amount of assisted gas flow to the build chamber through the inlet nozzle.

Samples are only printed in the extreme corner of the build plate (sample number 1, 6, 31,36). The layout of the print plate is shown in Fig. 12 (A).

Assisted gas inlet nozzles are present in the outer right side of the build chamber for Concept Laser Mlab Cusing Machines. Fig. 12(B) shows the position of assisted gas nozzle adjustment setup outside the build chamber. These nozzles can be adjusted individually, changing the amount of gas flow to the chamber by tightening or loosening the screws, which are shown in Fig. 12 (B).

The first set of samples is printed with nozzle closest to the chamber window (bottom of the build plate) having maximum assisted gas flow and the one farthest away (top of the build plate) with minimum assisted gas flow. The second set is printed with nozzles adjusted with a maximum assisted gas flow in the nozzles farthest away (top of the build plate) and least in the nozzle nearest to the chamber window (bottom of the build plate). Maximum assisted gas flow means that the nozzle is entirely open (100%), and minimum assisted gas flow is achieved by opening the nozzle by only 10%. The details on the nozzle adjustment are provided in Table 3.

This section presents the results to confirm the effect of assisted gas

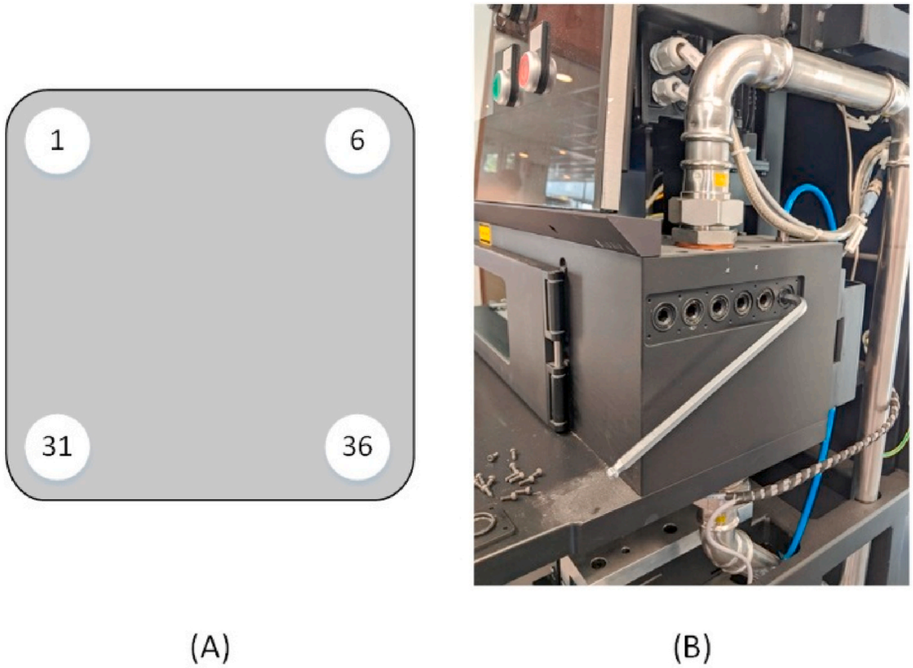

Fig. 12. Layout of samples in build plate, (b) Adjustable inert gas nozzle adjustment outside the build chamber.

Table 3
Nozzle adjustment for assisted gas flow in the chamber.

	Nozzle Opening	
Nozzle Number	Sample set 1	Sample set 2
1 (Nearest to build chamber window)	100%	10%
2	82%	28%
3	64%	46%
4	46%	64%
5	28%	82%
6 (Farthest from build chamber window)	10%	100%

on the dimensional deviations. Fig. 13 presents the "circularity" observations, which are the differences between the average parallel measurements and the average perpendicular measurements for each sample position. It means that the smaller value for circularity, the higher dimensional accuracy. The results from Fig. 13 (A and B) show that the circularity value decreases (better dimensional accuracy) as the pressure of the assisted gas decreases on the top row (low in blue and high in orange). Clearly, there is another effect that is influencing the build behavior from top to bottom rows, which can be related to the distance of the samples versus the chamber windows and atmospheric conduction that was explained by the rheology of the meltpool.

Furthermore, Fig. 13 (C and D) show that the circularity values increases as the pressure of the assisted gas increases on the bottom row (high in blue and low in orange) that shows less dimensional accuracy.

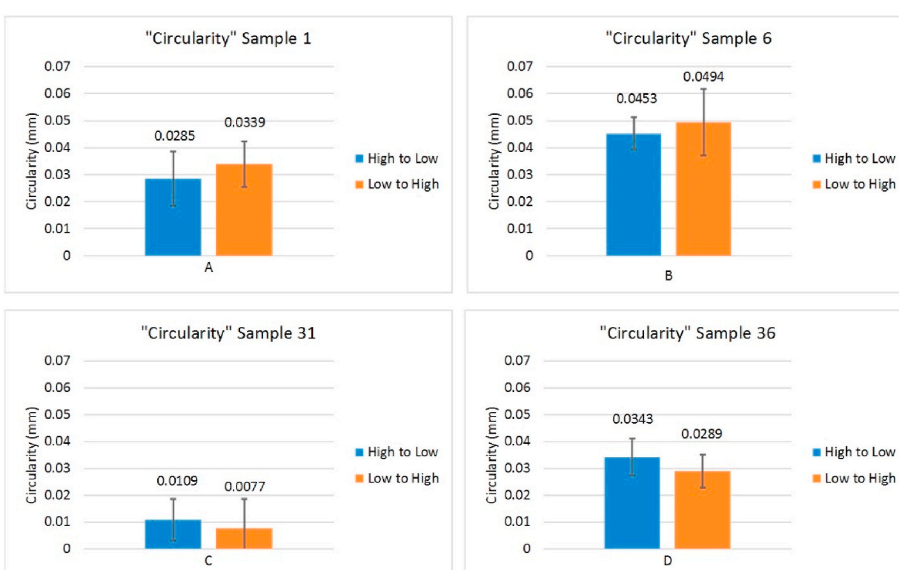

Fig. 13. Results of the gas adjustment verification experiment for Samples 1, 6, 31, and 36 showing the difference between the parallel and perpendicular diameters ("ovality") for both "high to low" and "low to high" process parameter sets.

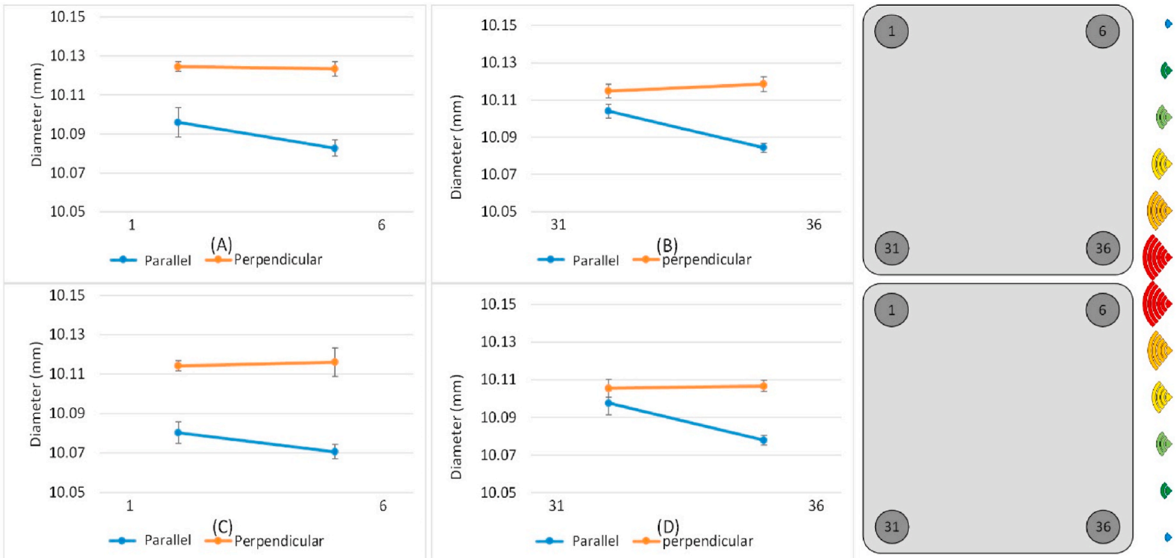

Fig. 14. Results of the gas adjustment verification experiment for Samples 1, 6, 31, and 36 showing the parallel and perpendicular diameters for both "high to low" and "low to high" process parameter sets.

This is the same trend as Fig. 13 (A and B) and shows the parallel and perpendicular diameters slightly diverge as the assisted gas is transitioned from 10% to 100% from the first nozzle to the last nozzle.

Sample 31 showed the most circularity for our previous test, and similar results were observed in this validation of experimental data. When the highest and lowest gas pressure was selected, the difference between diameters for sample 31 from ten measurements was obtained 10.9 and 7.7 μm, respectively. This shows higher pressure of the assisted gas increases the difference of parallel and perpendicular diameters (for about 41.5%). For sample 36, increasing the pressure of the gas increases the difference between diameters from 28.9 to 34.3 μm (Fig. 14).

This research has shown that assisted gas can change the performance of the LPBF process and may negatively affect the dimensional accuracy. However, it mainly indicates that further work is needed to explain the differences seen across the build plate if high-resolution accuracies are needed for industrial-scale printing.

Fig. 14 shows that the value of circularity is less (higher dimensional accuracy) for the samples printed in the rows, which are closer to the chamber window compared to the ones printed farthest. This could be explained by the fact that samples near to the chamber window have a better cooling effect, and this results in less dimensional deviation and increased circularity.

6. Conclusions

The study provides ample evidence on the effect of shrinkage based on the position of samples on the build plate in LPBF. Dimensional deviations of the printed samples is related to the flow and pressure of the assisted gas and sample position on the build plate. The conclusions drawn from the finding of the experiments are:

- The direction of the assisted gas flow inside the build chamber appears to have a secondary effect on the dimensional deviations.
- The positioning of samples with respect to the assisted gas nozzle influences the shape in terms of the dimensional accuracy. Samples printed close to the assisted gas nozzle (Rightmost along x-direction) exhibit maximum dimensional deviation from the nominal dimension, which is due to the pressure of the assisted gas. Moving further away from the nozzle along with the x-direction results in samples with higher accuracy close to the nominal dimension. This is related to the divergence effect of assisted gas, causing to produce circular samples.
- To achieve higher dimensional accuracy, it is recommended to have a uniform flow rate and pressure of assisted gas along with all the areas of the build chamber.
- Best results or least dimensional deviation occur in samples printed close to the window of the build chamber, which is explained by the cooling effect from the surrounding through the chamber window resulting in faster cooling and better circularity.
- It is crucial to consider the positioning of the chamber window while printing samples, as it supplements the cooling process and has an effect in the final shape of the samples.

Declaration of competing interest

None.

References

[1] Gibson I, et al. Additive manufacturing technologies. third ed. Springer; 2020.
[2] King WE, et al. Laser powder bed fusion additive manufacturing of metals; physics, computational, and materials challenges. Appl Phys Rev 2015;2(4):041304.
[3] Khorasani AM, et al. Production of Ti-6Al-4V acetabular shell using selective laser melting: possible limitations in fabrication. Rapid Prototyp J 2017;23(1).
[4] Rupal BS, et al. Geometric tolerance and manufacturing assemblability estimation of metal additive manufacturing (AM) processes. Materials & Design; 2020. p. 108842.
[5] Ameta G, et al. Tolerance specification and related issues for additively manufactured products. In: ASME 2015 international design engineering technical conferences and computers and information in engineering conference. American Society of Mechanical Engineers; 2015.
[6] Alvarez P, et al. Computationally efficient distortion prediction in powder bed fusion additive manufacturing. Int. J. Eng. Res. Sci 2016;2(10):39–46.
[7] Chen Y, Vastola G, Zhang YW. Optimization of inert gas flow inside laser powder bed fusion chamber with computational fluid dynamics. In: Solid freeform fabrication 2018: proceedings of the 29th annual international; 2018.
[8] Królikowski M, Filipowicz K. Verification of geometrical accuracy of selective laser melting (SLM) built model/sprawdzanie dokładności modelu wytworzonego metodą selektywnego topienia laserem. Adv Manuf Sci Technol 2013;37(3):85–91.
[9] Kamarudin K, et al. Dimensional accuracy and surface roughness analysis for AlSi10Mg produced by selective laser melting (SLM). In: MATEC web of conferences. EDP Sciences; 2016.
[10] Zhang L, et al. Horizontal dimensional accuracy prediction of selective laser melting. Mater Des 2018;160:9–20.
[11] Wang D, et al. Characteristics of typical geometrical features shaped by selective laser melting. J Laser Appl 2017;29(2):022007.
[12] Afazov S, et al. Distortion prediction and compensation in selective laser melting. Additive Manufacturing 2017;17:15–22.

[13] Yang Y, et al. Accuracy and density optimization in directly fabricating customized orthodontic production by selective laser melting. Rapid Prototyp J 2012;18(6):482–9.
[14] Qian M, et al. An analytical model for constitutional supercooling-driven grain formation and grain size prediction. Acta Mater 2010;58(9):3262–70.
[15] Gowri S, Samuel F. Effect of cooling rate on the solidification. Metallurgical Transactions A 1992;23(1):3369–76.
[16] Fu J, et al. Effect of cooling rate on solidification microstructures in AISI 304 stainless steel. Mater Sci Technol 2008;24(8):941–4.
[17] Irvine T. Heat transfer during solidification of layered intrusions. I. Sheets and sills. Can J Earth Sci 1970;7(4):1031–61.
[18] Manvatkar V, De A, DebRoy T. Heat transfer and material flow during laser assisted multi-layer additive manufacturing. J Appl Phys 2014;116(12):124905.
[19] Khorasani AM, et al. Mass transfer and flow in additive manufacturing of a spherical component. Int J Adv Manuf Technol 2018;96(9–12):3711–8.
[20] Khorasani AM, Gibson I, Ghaderi AR. Rheological characterization of process parameters influence on surface quality of Ti-6Al-4V parts manufactured by selective laser melting. Int J Adv Manuf Technol 2018;97(9–12):3761–75.